Discrete Numerical Modeling of Jointless Prestressed High Performance Concrete Bridges

P.K. Basu, Vanderbilt University, Nashville, TN
D.J. Knickerbocker, Vanderbilt University, Nashville, TN

ABSTRACT

The experimental results of three-year monitoring of the performance of two heavily instrumented jointless prestressed HPC bridges are evaluated by comparing with results predicted by computer-based discrete modeling using the finite element method. Modeling is undertaken in two stages. First, an individual pretensioned beam is modeled to study the effects of prestress, creep and shrinkage, self-weight, and construction loads during pouring of deck. Modeling of the bridge as a whole followed this including the effects of substructure components like abutments and supporting piles. The analysis results for temperature change, creep and shrinkage, and standard truck live loads are compared with the experimental ones and suitable recommendations are made to help modeling of jointless bridge behavior in a design office environment.

Keywords: HPC, Jointless, Prestressed bridge, Finite element, Temperature, Truck load

INTRODUCTION

The use of high performance concrete (HPC) coupled with jointless construction provides a unique combination of material and structural system to reduce the life cycle cost of highway bridges. This is possible because of prolonging the life of the bridge through reduced maintenance needs resulting from increased resistance against environmental and operational sources of deterioration coupled with reduced first cost due to the elimination of expensive bearings and expansion joints. This is further aided by structural efficiencies associated with stronger material and continuous construction.

The first logical step of jointless construction is to eliminate joints at the piers by replacing simple spans with continuous spans. Integral construction of the girder and deck system with the end abutments makes it fully jointless. These steps will require accounting for the secondary forces in the design, if large enough, due to constrained thermal expansion and contraction. Moreover, the possibility of additional secondary forces due to differential support settlements may have to be addressed. Under the sponsorship of State and Federal agencies, the authors have been undertaking extensive experimental and analytical investigation of two such bridges across State Rt. 840 in Dickson, TN, for more than three years. Of the many objectives of the investigation, this paper is primarily concerned with computer modeling and simulation of the bridge for evaluating the experimental findings as well as to have a better understanding of the behavior through parametric studies related to issues like

1. The response of substructure (abutments, pier, and pile supports) to changes in temperature as well as creep and shrinkage effects.
2. The response of superstructure to standard truck loads, especially with reference to the distribution of loads between the girders and the effect of continuity at the end abutments and the interior pier.
3. The effect of skew angle of such bridge on superstructure response, since both bridges have significant skewness.
4. The effect of movement of support system on the structural integrity of the bridge.

Before the aforementioned studies can be undertaken, it is important to create and validate the discrete numerical model to be used by comparing the analytical results with the experimental findings. Of the different discrete numerical methods, the finite element method is most matured and finds widest usage, both in research and practice. Due to ready availability, as well as previous successful experience in bridge modeling[1], the software ANSYS[2] with multi-physics capability was adopted for this study. Modeling was undertaken in two major stages – a) validation stage, and b) production stage. The validation stage enabled the selection of an optimal model, which represents the bridge system with a fair degree of accuracy and at the same time minimizes the model preparation time as well as computational effort. The latter is largely controlled by the size of the model; so, it is necessary to minimize the number of unknown variables in the model. If the selected model gives response quantities that agree with those measured in the field, it can then be used in the production stage for in depth understanding of the behavior of the candidate jointless HPC bridges under different external influences.

DETAILS OF CANDIDATE BRIDGES

The two-span bridges under study are located on Porter Road and Hickman Road and will be termed hereinafter as PR Bridge and HR Bridge. As shown in Fig. 1, the two-lane PR Bridge has two spans of 159 ft each. There are four pretensioned 72" deep bulb tee girders in each span, with flange and bulb widths equal to 40" and 26", respectively. As shown in Fig. 2, each girder has 54 strands (7-wire, uncoated, stress relieved, 0.6”ϕ, A_s = 0.217sq.in. and P_i = 43,943lb/strand) out of which 8 are unbonded near the ends, and six are raised near the ends. The longitudinal axis of the bridge has a skew angle of 26^{o}42'15". It may be noted that the abutment structure on the east side is taller but the piles are shorter, as compared to the ones for the west abutment.

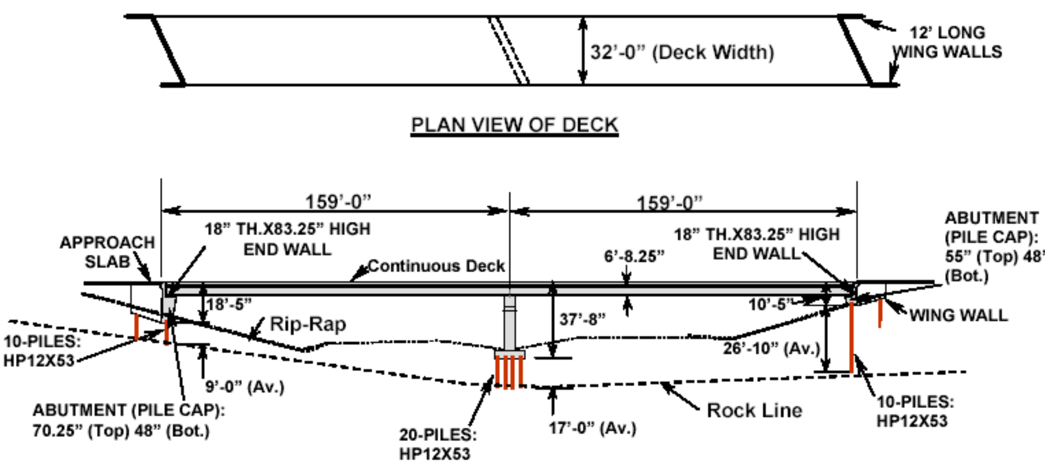

Fig. 1 North Elevation of PR Bridge

As shown in Fig. 3, the two-lane HR Bridge has two spans of 139'-4" (north) and 151'-4" (south). As in the case of PR Bridge, this bridge also has four pretensioned girders with cross-sectional dimensions same as those for PR Bridge. In this case, however, four fewer strands are used out of which six are partially unbonded, and six draped. The longitudinal axis of the bridge has a skew angle of 17^o-32'-16". It may be noted from Fig. 3 that the abutment structure and supporting piles at the two ends are almost of same size.

The superstructure of the bridges was constructed in two stages. First, the pretensioned girders for individual spans were cast in a precast products factory, transported to the bridge site and placed on the substructure, which was constructed earlier. This was followed by integrated casting of continuous deck slab, end walls of the abutments, diaphragm at the pier and girder ends. Limited continuity with the girder ends was achieved through rebars projecting from the web and flange at girder ends, see Fig. 4. In other words, the

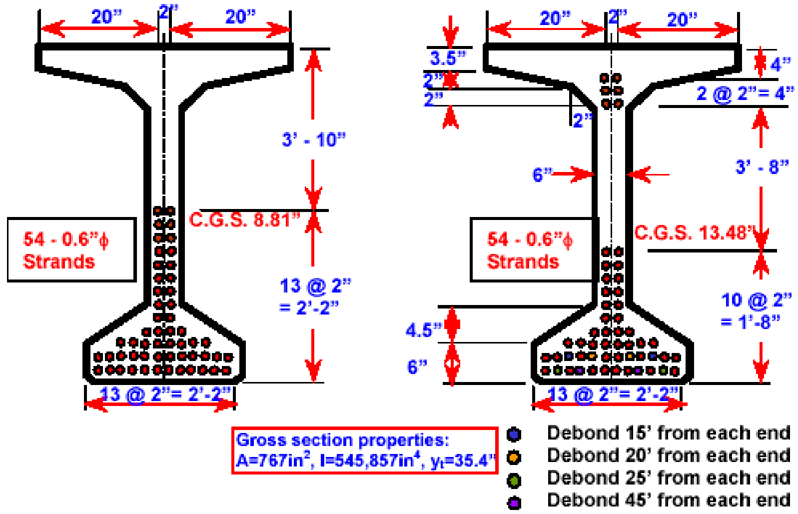

(a) Midspan Section (b) End Section

Fig. 2 Typical midspan and support sections of PR Bridge girders

construction details allowed for full continuity for the deck slab but limited continuity for the precast girders. Different grades of concrete were used in girders, deck, and substructure. The steel foundation piles were of size HP12x63. The average mechanical properties of concrete were as shown in Table 1. The strength values are based on tests. Other mechanical properties of concrete were measured for concrete used in the girders only.

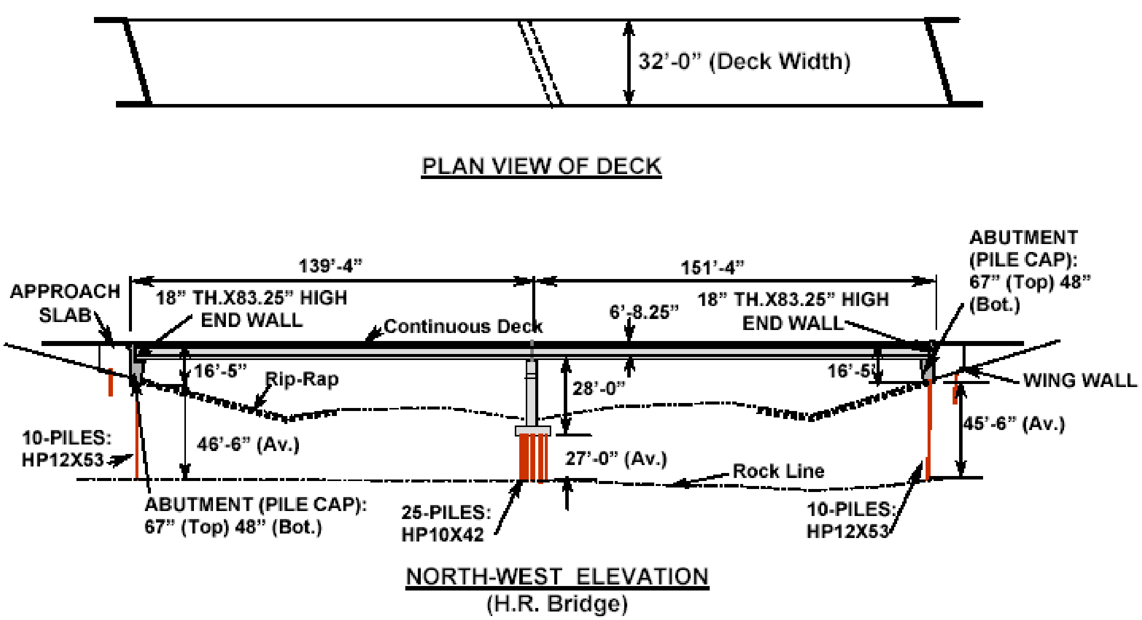

Fig. 3 West Elevation of HR-Bridge

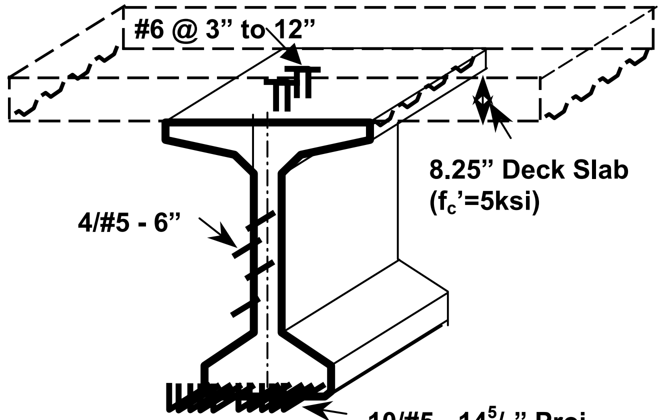

Fig. 4 Projected rebars from girder end

Table 1: Average Properties of Concrete for PR- and HR-Bridge

Component	f_c', psi	f_t', psi	E_c, psi
Girders	10,530	926	6,594,267
Deck	7,964	762	4,500,568
Substructure	6,457	626	4,459,734

MODEL CREATION & VALIDATION

Here the objective is to come up with the simplest possible model with the least loss of accuracy. Modeling the post-tensioned girders is complicated by the fact that apart from concrete, it is necessary to model the steel strands and the rebars. Explicit modeling of all the components will require a very high-resolution model. Moreover, apart from allowing for widely different mechanical properties of the three component materials, it is necessary to allow for force transfer by bond between steel (particularly the strands) and concrete. This is especially true if the objective of analysis includes consideration of crushing and cracking of concrete, say, when the tensile strain reaches a limiting value, as well as bond slippage. Further complications are introduced if the nonlinear behavior of concrete including creep and shrinkage phenomena and strain-hardening behavior of steel are also accounted for. In reality, the model should be of right resolution to achieve the objectives of the analysis with a reasonable degree of accuracy. In order to achieve the right model resolution, it may be instructive to clearly identify the objectives of the analysis affecting the choice of finite element model. These are

1. Performance of the jointless construction under changes in temperature – if the analysis is undertaken for normal range of temperature change, nonlinear behavior

may not be an issue. However, cracking of concrete in some critical locations may occur and the model should be able to handle it. In this case however, the role of lateral deformation of the foundation piles may be important and it is necessary to allow for the resistance offered by the surrounding soil against such movement.
2. Effect of creep and shrinkage on deformations and stresses in the bridge - In order to get a reasonable qualitative understanding of these phenomena, it may be recognized that these affects are akin to thermal effect in the sense that these can be treated as initial strain effects. So, it may not be necessary to use special models to allow for creep and shrinkage effects.
3. Effect of live load on bridge behavior, especially with respect to load distribution between the supporting girders in the context of jointless construction. This does not require any more refined model than what is needed under objective number 1.
4. Determinations of the nature of movement at the skew supports caused by temperature changes as well as live loading on the bridge. This does not require any special treatment, except that support conditions at the abutments and the pier should be defined accurately. It may be noted in this context that although the deck slab has full continuity, the girders have only partial continuity.

The factors that require special attention in discrete numerical analysis of reinforced concrete structures[3] are

- Constitutive laws for steel reinforcement and prestressing strands (elastic, strain-elastic-hardening, or elastic-plastic)
- Constitutive laws for concrete (linear elastic, nonlinear elastic, or elastic-plastic)
- Limit or failure surface for concrete (three or five-parameter model[4,5])
- Modeling of steel reinforcement (discrete, embedded, or smeared[6])
- Modeling of prestressing strands (discrete with prestrain including allowance for bond length development)
- Modeling of cracks in concrete (discrete, or smeared)
- Bridging effect of rebars across cracks.
- Modeling of bond-slip at steel/concrete interface including tension stiffening

The commonly used limit surface (or failure envelop) for tri-axial behavior of concrete in compression is due to Williams and Warnke[4,5]. In tension, the failure criterion is defined in terms of a damage parameter. Tension softening of concrete is modeled with a smeared crack approach. Modeling of structural elements considering the steel-concrete relative slip requires an understanding of the existence of bond stress at the interface resisted by adhesion, friction, and interlock between the bar ribs and concrete[7]. Due to relative slip with surrounding concrete, a bar in tension transmits stresses to the surrounding concrete. Under high enough stress, cracks form in the concrete, which eventually propagate to the surface. Based on experimental observation, bond stress vs. slip relationships for the progressive development of micro-cracks in the concrete have been put forward. Often, concentrated bond link elements are introduced at the nodes, connecting concrete and steel. Ngo and Scordelis[8] first proposed such elements represented by orthogonal springs. Such model is often limited to elastic constitutive law. The inter-facial bond between concrete and steel elements can be visualized as shown in Fig. 5. It consists of two nodes, say, i and j, with identical coordinates and orthogonal springs. This element does not have any physical dimensions. If, however, damage initiation and propagation is not an issue, the most common approach for finite element modeling of reinforced concrete members relies on the simplifying assumption of a perfect bond between steel and concrete.

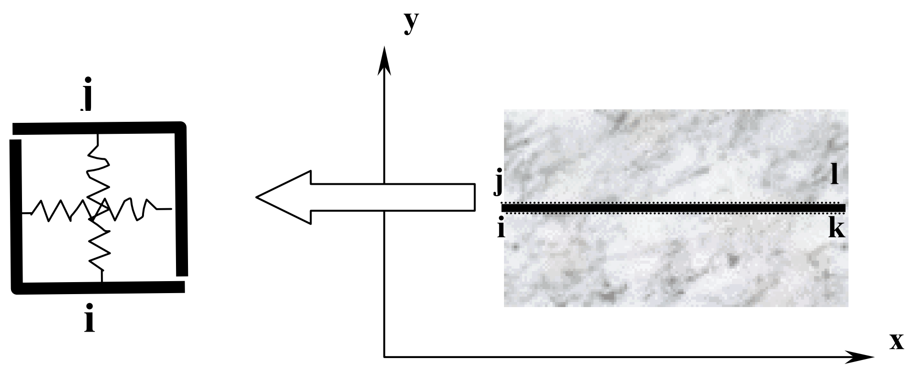

Fig. 5 Bond-Link Element

Some of the above requirements are available in a number of general-purpose software like ANSYS[2], ABAQUS[9], ADINA[10], and DIANA[11]. DIANA is relatively a recent software from Europe and, perhaps, is best suited to model reinforced concrete. However, due to built in capabilities and long-term reputation, ANSYS is the most widely used software for modeling major concrete structures.
With ANSYS, the concrete can be modeled by a eight nodded solid element (with three degrees of freedom at each node) designated as SOLID65 which allows a smeared crack analogy for the tension zone, crushing based on a five parameter William and Warnke[4] model and plasticity based on the Drucker-Prager loading function is used to calculate multi axial effects of the stress. So, with this element, the concrete material is capable of directional integration point cracking and crushing besides allowing for plastic and creep behavior. The five parameters of William-Warnke failure criterion are as follows:

- Maximum Uniaxial tensile strength
- Maximum Uniaxial compressive strength
- Maximum biaxial compressive strength
- Maximum biaxial confined pressure stress
- Maximum biaxial strength for uniaxial pressure

Actually, the cracking and crushing checks are performed at each of the eight integration points in the element. Unless the specified tensile or compressive strength are exceeded by one of the principal stresses at an integration point, the behavior is elastic. Otherwise, cracked or crushed regions are formed orthogonal to the principal stress direction leading to redistribution of stresses. Due to the resulting nonlinearity, an iterative solution algorithm needs to be followed.

Apart from the matrix material (e.g. concrete) it can handle additional three different materials (e.g. up to three independent reinforcing materials) within each element. A part or all of the reinforcement, which has uniaxial stiffness only, can be smeared throughout the solid element, the directional orientation being accomplished through user specified angles. The limitation is that the sum of the volume ratios for all rebars must not be greater than 1.0. The remaining rebars and prestressing tendons can be modeled by axial bar elements (LINK8). In the case of prestressing tendons, additional consideration needs to be made to allow for initial strain due to prestress. Bond-slip and tension stiffening in the case of discretized rebars and prestressing tendons can be modeled by using bond-link elements or spring elements (COMBIN14) with elastic or elastic-plastic properties.

FINITE ELEMENT MODELING OF PRETENSIONED GIRDER

The length of precast PR Bridge girders are 156 ft (47.5 m) each, and that for an instrumented HR Bridge girder is 148 ft 8 in. (45.3 m). The gross cross-sectional area and moment of inertia of the girders about the strong axis are A = 767 in.^{2} (4948 cm^2) and I_x = 545,857 in.^{4} (0.227 m^4). To arrive at an appropriate finite element model for the girders, detailed three-dimensional modeling of a PR Bridge girder was considered by explicitly allowing for concrete, rebars, and prestressing strands. The software chosen for the purpose was ANSYS 6.1 running under Solaris O.S.

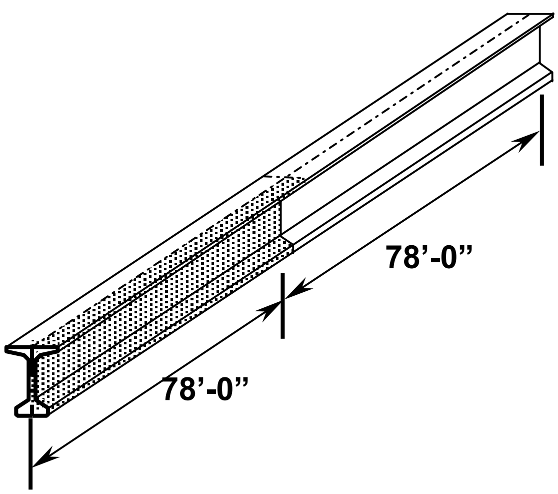

(a) Shaded quadrant was modeled

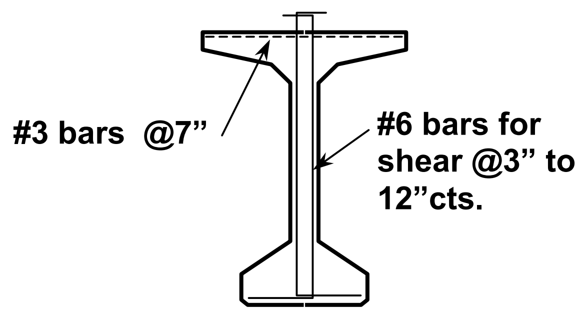

(b) Rebar details

Fig. 6 Modeled Segment of Girder

Assuming that the response of the girder will be symmetrical about its vertical axis of geometric symmetry in the cross-section, as well as with respect to its centerline over the span, only one-fourth of the girder with respect to these axes is considered, as shown in Fig. 6. So, taking advantage of 2-way symmetry, only one quadrant of the girder was modeled using SOLID65 three-dimensional elements to represent the concrete as well as the reinforcing bars that were not discretized and were smeared instead. As mentioned above, the element is nonlinear and requires an iterative solution. In the event, both cracking and crushing are used together; it is necessary to apply the load slowly to prevent possible fictitious crushing of the concrete before proper load transfer can occur through a closed crack. Based on average test data, the elastic modulus for concrete was taken as 6.5×10^6 psi (44827.6 Mpa) and Poisson's ratio = 0.1.

The shear reinforcement was modeled by LINK8 elements. The same element type was used to model the strands as well. Different models were tried to represent the bond effect in discretized rebars and strands as well as the development of prestrain in the strands. Based on a prestressing force at transfer = 43,943 lb. (195.3 kN) and $E = 29 \times 10^6$ psi (2×10^5 Mpa), the initial maximum strain in a strand = 0.007.

The analysis was undertaken with different levels of sophistication achieving different levels of success, as described below.

1. The simplest beam model consisted of SOLID65 elements for concrete and LINK8 elements for strands with no allowance for rebars, bond-slip, and harped strands. The computed camber value due to prestress was significantly more than the observed value.

2. In the next model the harping of strands was incorporated leading to slight lowering of predicted camber value.

3. In the following improvement of the model, the interface behavior between the concrete and prestressing strands as well as rebars were modeled using COMBIN14 spring elements with coincident nodes. Appropriate constitutive properties were assigned to these elements to capture the effect of bond and bond-slip. At each node of LINK8 elements two such spring elements, one parallel and the other perpendicular, were used. Using this model the girder behavior showed excellent agreement with measurements. However, graphical display of deformed shape appeared confusing due to the COMBIN14 elements constrained to undergo axial deformation only.

4. In order to avoid the visualization problem experienced in the last model, the bond-slip elements were assigned a very small but finite length resulting in non-coincident nodes. But this change led to worsening of the performance of the model.

5. Finally, a model, shown in Fig. 7, consisting of SOLID65 concrete elements incorporating smeared representation of transverse steel was used. In addition, the 0.6" dia. prestressing strands and 0.75" dia. shear reinforcement were represented by LINK8 elements, assuming perfect bond with concrete. In the girder cross-section, the prestressing strands are located at 2-in (50.8 mm) centers in both directions, so it was found to be convenient to discretize the cross-section by a 2"x2" element mesh. Along the length of the girder both concrete and strand elements measure 3 in (76.2 mm). The bond-slip effect in prestressing strand was accounted for by calculating the transfer length of the strands and ensuring that the prestrain

varied linearly from zero value at the end to its full value over this length. Instead of using AASHTO/LRFD Bridge Specifications[12] formula, it was found to be more reasonable to estimate the transfer length using the formula proposed by Mitchell[13] et al. for use with high strength concrete as

$$\ell_t = 0.33 f_{pi} d_b \sqrt{\frac{3}{f'_{ci}}} \tag{1}$$

in units of ksi and in., where stress in the strand immediately after transfer f_{pi} = 185 ksi (1.28 GPa), strand diameter d_b = 0.6 in. (15 mm), concrete compressive strength at release f'_{ci} = 8 ksi (55 MPa), and resulting estimated l_t = 24 in. (610 mm).

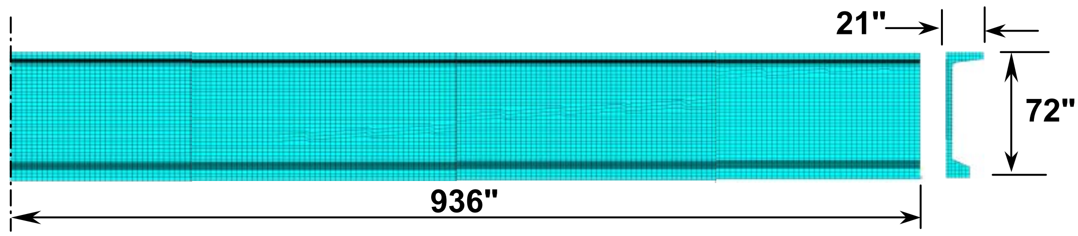

Fig. 7 Three-D Finite Element Model of Prestensioned Girder

This model led to all-around improvement of results when analysis was undertaken to simulate the casting stage, curing stage in the storage yard, temperature changes, and external loading during deck construction.

Camber Check

Camber, deflection, and stress values showed good agreement with the measured data. The predicted and computed camber values are compared in Table 2. PI and PE refer to interior and exterior girders.

Table 2. Measured and predicted camber at relevant stages of construction of PR-Bridge

	Transfer	Initial Storage	Deck Load
Beam Theory	3.61”	4.80”	0.61”
FEA	3.39	4.51	0.43
Measured (PI)	2 ½	5	¾
Measured (PE)	3	4 ¾	1 $^1/_8$

For simulation of thermal effect, a particular case of temperature change from morning to afternoon on a particularly hot day was analyzed. The nonlinear thermal gradients of temperature difference in each of the four girders studied approached 40ºF (22ºC) difference at the top, and only about 5ºF (3ºC) at the bottom. Curvature changes imposed by these temperature gradients led to an average change in camber of 0.76 in. (1.9 cm), a significant percentage of the initial measured cambers of about 3 in. (7.6 cm).

Peak Stress Check

Current code requirements (ACI, 1999) specify stress limits in prestressed members in compression as

$$\sigma_c = 0.60 f_{ci}^{'} \tag{2}$$

and in tension (at the ends of the member),

$$\sigma_t = 6\sqrt{f_{ci}^{'}} \tag{3}$$

With $f_{ci}^{'} = 8{,}000$ psi, the above limits are $\sigma_c = -4{,}800$ psi, and $\sigma_t = 536$ psi. Extreme fiber stresses in the girder can be calculated by simple beam theory accounting for flexure and axial effects. Table 3 presents the stresses calculated in this manner from the maximum negative moment conditions found in the casting bed at transfer, and in the storage yard, compared with maximum bending stresses computed by FEM analysis. In simple beam theory calculations, sections of maximum effects at transfer were located at transfer length of 24 in. (61 cm) from the ends, and in storage yard, at support locations.

Table 3. Maximum stresses predicted by simple beam theory and FEM(1 psi = 6.9 kPa)

Condition	Beam Theory		FEM	
	P_{max}	P_{min}	P_{max}	P_{min}
Transfer	-69	-4,804	-30	-4,793
Storage	195	-5,075	257	-5,475
ACI limit	≤ 536	≥ -4,800	≤ 536	≥ -4,800

At transfer, the stresses satisfy code limitations. But in storage with supports moved inwards, the compressive stress exceeded the limiting value by about 14%. In general, the simple beam theory and FEM results seem to be in reasonable agreement.

In order to reduce the unknown degrees of freedom of the model, a series of studies were undertaken with one-dimensional model of the beam. This model consisted of 39 BEAM4 elements with all the strands modeled by the same number of LINK8 elements. Area of the strand element was reduced, as needed, to represent the unbonded segments. The end nodes of LINK8 elements were coincident with the centroidal line of the effective strand areas. Perfect bond was assumed between strand and concrete. At each of the 40 nodal sections, the beam nodes were tied to the strand nodes by vertical rigid link elements. The viability of this one-D element as compared to the three-D model considered earlier was thoroughly checked under transfer condition and under deck weight. The thermal load solutions based on the 3-D model are shown Fig. 8.

After the simulations described above, the final beam model was implemented into the PR Bridge model, which further proved the approach to be viable through a series of simulations, as discussed in the following.

BRIDGE MODEL

MATERIAL PROPERTIES

Concrete: Material properties like compressive strength, tensile strength, and modulus of elasticity used in the model were based on laboratory tests of concrete specimens made at the construction site. Average 28-day compressive strength of the girder concrete was found to be close to 10,000 psi (68.9 MPa), and that of the deck: 7,000 psi (48.3 MPa). Mean 28-day tensile strength of girder and deck concrete based on split cylinder test were 900 psi (6.2 MPa) and 700 psi (4.8 MPa), respectively. Based on laboratory tests, the modulus of

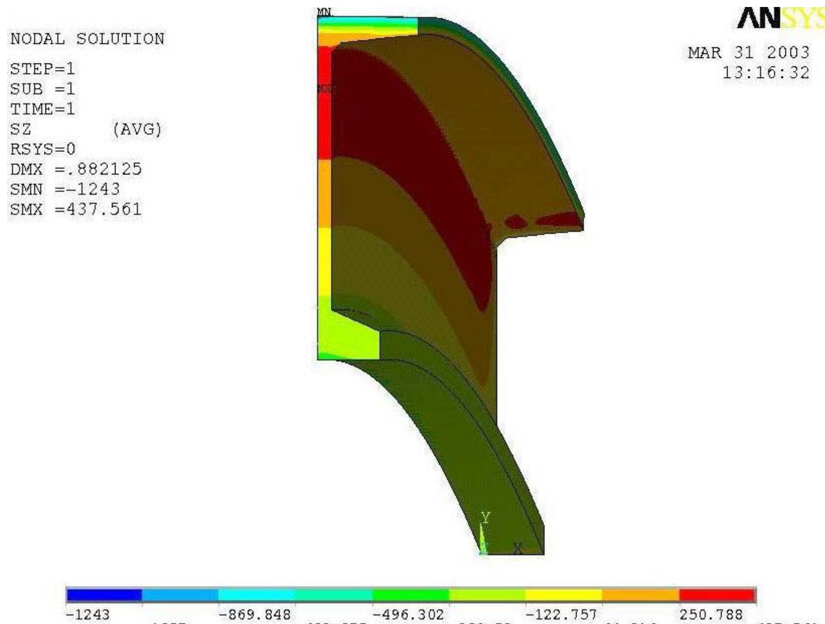

Fig. 8 Thermal Stresses by Three-dimensional Model

elasticity for girder concrete and deck concrete were found to be about 6,500 ksi (44.8 GPa), and 4,500 ksi (31 GPa), respectively. In the case of substructure (abutments, piers, etc.), at 28-days, the concrete had a compressive strength of 5,000 psi (34.5 MPa), tensile strength of 700 psi (4.8 MPa), and elastic modulus of 4,500 ksi (31.0 GPa).

Backfill and Soil: The end abutments provide lateral support to sandy backfill material, which carries surcharge load from the approach slab as well. The steel piles (HP 12x53) used in the foundation were driven mostly through sandy clay till refusal, when rocky stratum (limestone) was encountered. The resistance against movement of the abutment offered by the granular backfill material as well as that offered by sandy clay against the foundation pile requires proper representation. Although the backfill material and the foundation soil act as semi-infinite continuum, the common practice is to use the Winkler model. This simple model replaces the soil by a grid of isolated springs; the property (or stiffness coefficient) of a spring is based on the property of backfill or foundation soil material in the vicinity and its depth below the top surface. For a given backfill material (say, dense, medium dense, or loose), the force P in the equivalent backfill springs corresponding to a δ-value can be calculated by $P = K\gamma z A_T$. The stiffness coefficients, K, were estimated using data provided by NCHRP[14], and adjusted according to depth and the tributary area associated with the equivalent spring. Fig. 9 presents NCHRP variation of spring stiffness, K, with horizontal displacement, δ. In the formula for P, $\gamma =$ density of backfill material; $z =$ depth of point below top of backfill; and $A_T =$ tributary area of the nodal point on the back of abutment wall. Based on this formula, the P-δ curves for the springs were obtained, as shown in Fig. 10.

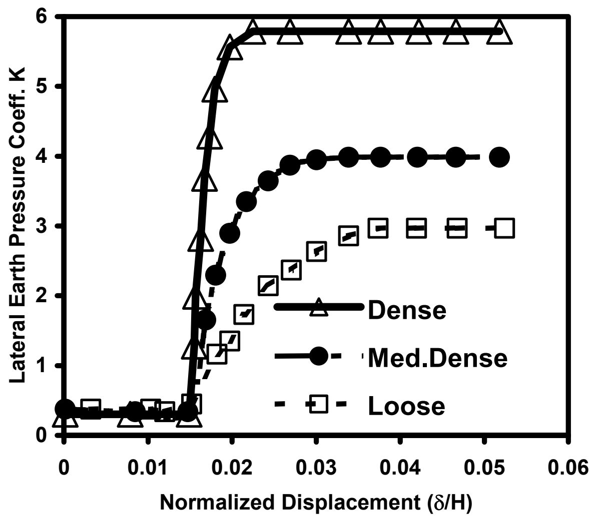

Fig. 9 NCHRP Lateral Earth Pressure Coefficient vs. Horizontal Displacement

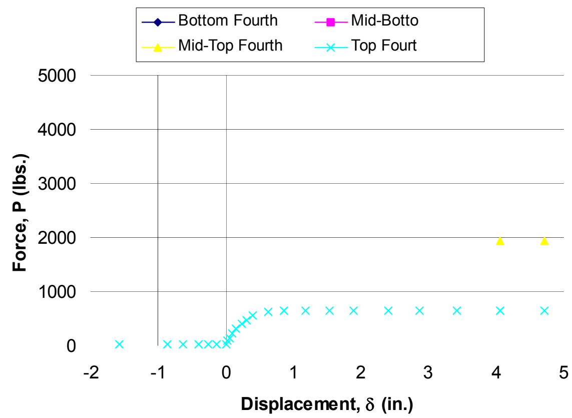

Fig. 10 Force Deflection Curves for 1 sft (0.09 m^2) of Backfill, (NCHRP, 1991)

Passive resistance against pile translation was modeled using ANSYS nonlinear spring elements COMBIN39, the properties of which were based on Fig. 10. In doing so, pile-soil-pile interaction effects[15] were ignored. The unidirectional springs were placed to resist forward, backward, and sideways translation of the piles. Soil reaction against concrete surfaces of abutments, back walls, and wing walls was modeled with adjustment to soil stiffness elements according to associated tributary areas.

GEOMETRY

Piles**:** The steel piles in the abutment foundation were modeled using the thin-walled plastic beam element BEAM24, which allows exact definition of cross-section allowing nonlinear plastic behavior. For the purpose of this preliminary study all piles are modeled as 30 ft (9.1 m) long, discretized into 1-ft long elements, with fixity enforced at the 30-ft depth.

Abutments, etc.: The 8-node concrete element SOLID65 was used again to simulate the abutments, back walls, diaphragm, pier, and deck. As was mentioned before, this element is specifically designed to handle reinforced or plain concrete behavior, and includes capability to simulate cracking and crushing. Reinforcement was modeled as “smeared” throughout the element, requiring input of a reinforcement volume ratio in each direction. In the isometric view of the model in Fig. 11, different density of reinforcement is indicated by different color. It may be noted that the amount of steel in the deck increases toward the central pier to resist the negative moment induced there. As shown in Fig. 11, two interior support models were considered. For proper definition of support condition, pier modeling was found to be essential.

The precast girders were simulated using the 2-node elastic beam element BEAM4, with nodes located on the centroidal line. Thus, the 156-ft (47.5-m) girders were uniformly discretized by 2-ft (0.6-m) long elements. BEAM4 elements with very high stiffness were used at 2-ft spacing as “rigid links” connecting the nodes of the deck elements lying above the girder centerline with the girder nodes, as shown in Fig. 12. These “rigid link” elements are also used at the ends of the girders to connect the beams to the top and bottom of the end wall. The “roller” support at the pier/diaphragm interface is modeled via embedded anchor bolts through the centerline of the pier and diaphragm, again using the element type BEAM4, along with spring elements at the interface to simulate the existence of relatively low resistance to rotation there. The model also implements the wing walls, including the supporting piles in the same manner as the rest of the abutment components.

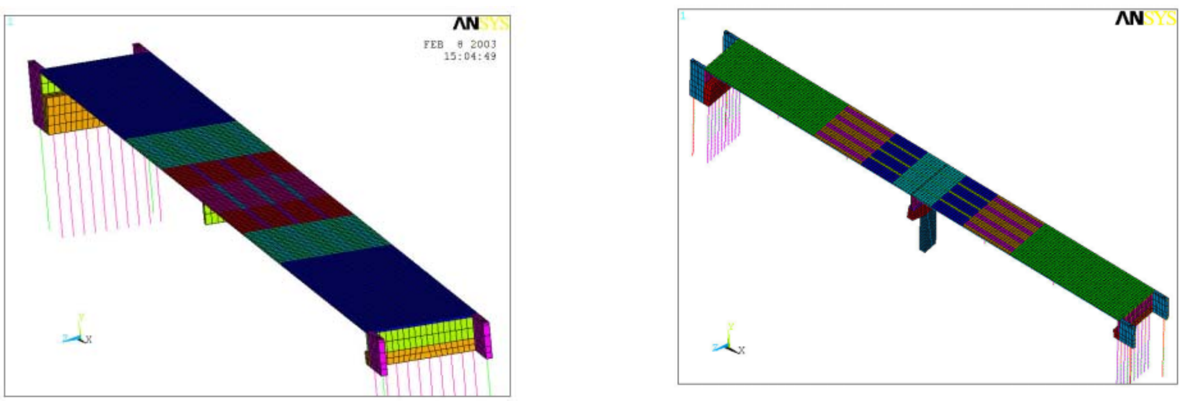

(a) Pier replaced by simple support (b) With pier modeled as is

Fig. 11 ANSYS Model for the Full Bridge

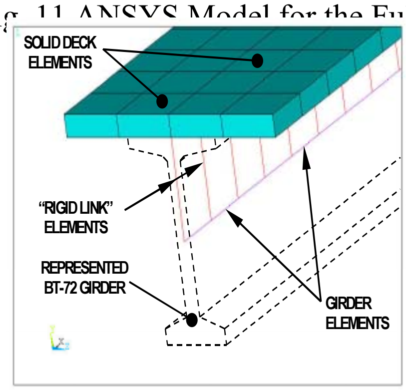

Fig. 12 Modeling of rigid link connection between deck slab and precast girder

THERMAL LOADING OF SUPERSTRUCTURE

The distribution of temperature along the depth of a concrete bridge superstructure is markedly nonlinear. The design guidelines[17] recommends an approximate stepwise linear temperature gradient. This gradient is presented in Fig. 13(a), where the zero value corresponds to the "base" temperature that loosely corresponds to the ambient temperature. If this temperature profile were imposed upon a tributary composite section of the bridge with width profile as shown in Fig. 13(b) in which the deck width is reduced according to the transformed section stiffness ratio

$$n = \frac{E_{deck}}{E_{girder}} = \frac{4500\,\text{psi}}{6500\,\text{psi}} = 0.69 \tag{4}$$

it would induce axial and bending strains according to

$$\varepsilon_{\circ} = \frac{1}{A}\int_{y_b}^{y_t} \alpha \Delta T(y) b(y) dy \tag{5-a}$$

$$\phi = \frac{1}{I}\int_{y_b}^{y_t} \alpha \Delta T(y) b(y) y dy \tag{5-b}$$

in which cross-sectional area of the transformed section A = 1380 in.^{2} (8903 cm^2), y-axis ordinate at top of section y_t = 28 in. (71 cm), and at section bottom y_b = -53.75 in. (-136.5 cm), coefficient of thermal expansion $\alpha = 5.5 \times 10^{-6}$, and $\Delta T(y)$ and $b(y)$ are the thermal gradient and width function, respectively, along the y-axis. The strain $\varepsilon_{\circ} + \phi \cdot y$ resulting from the AASHTO design gradient is presented in Fig. 13(c). The problem with applying thermal loading to the FE model is that thermal gradients can be induced in the current setup only in a piecewise linear variation with depth: one through the deck, and the other the precast girder. Simulation of a given thermal gradient therefore involves choosing temperature values T_1 at the bottom of the girder, T_2 at the girder/deck interface, and T_3 at the top of the deck, introducing least possible error in resulting thermal effects. In order to ensure that the resulting strains are the same, the centroidal strain and curvature values given by Eq. (5) based on the "actual" thermal gradient $\Delta T_{actual}(y)$ be same as those for simulated approximation $\Delta T_{FE}(y, T_1, T_2, T_3)$ for the model, so that:

$$\int_{y_b}^{y_t} \Delta T_{actual}(y) b(y) dy = \int_{y_b}^{y_t} \Delta T_{FE}(y, T_1, T_2, T_3) b(y) dy \tag{6-a}$$

$$\int_{y_b}^{y_t} \Delta T_{actual}(y) b(y) y dy = \int_{y_b}^{y_t} \Delta T_{FE}(y, T_1, T_2, T_3) b(y) y dy \tag{6-b}$$

Solving Equations 6 for, say T_2 and T_3 in terms of T_1 leaves one unknown value. To calculate T_1, the difference between the actual and approximate stress profiles based on Eq. (7) can be minimized with respect to T_1.

$$\sigma(y) = \varepsilon_{\circ} + \phi \cdot y - \alpha \Delta T(y) \tag{7}$$

The minimization equation can be written as

$$\frac{d\left[\Delta T_{actual}(y) - \Delta T_{FE}(y, T_1, T_2, T_3)\right]}{dT_1} = 0 \tag{8}$$

In Fig. 13(c) is presented the gradient derived for simulating the AASHTO-proposed design gradient, and the difference in resulting stress is shown in Fig. 13(d). In Fig. 13(e-h), four cases of measured thermal gradient are presented in terms of enforced strain $\alpha\Delta T_{actual}$, along with resulting axial and bending strain $\varepsilon_{\circ} + \phi \cdot y$, and "equivalent" imposed strain $\alpha\Delta T_{FE}$ used in the analysis.

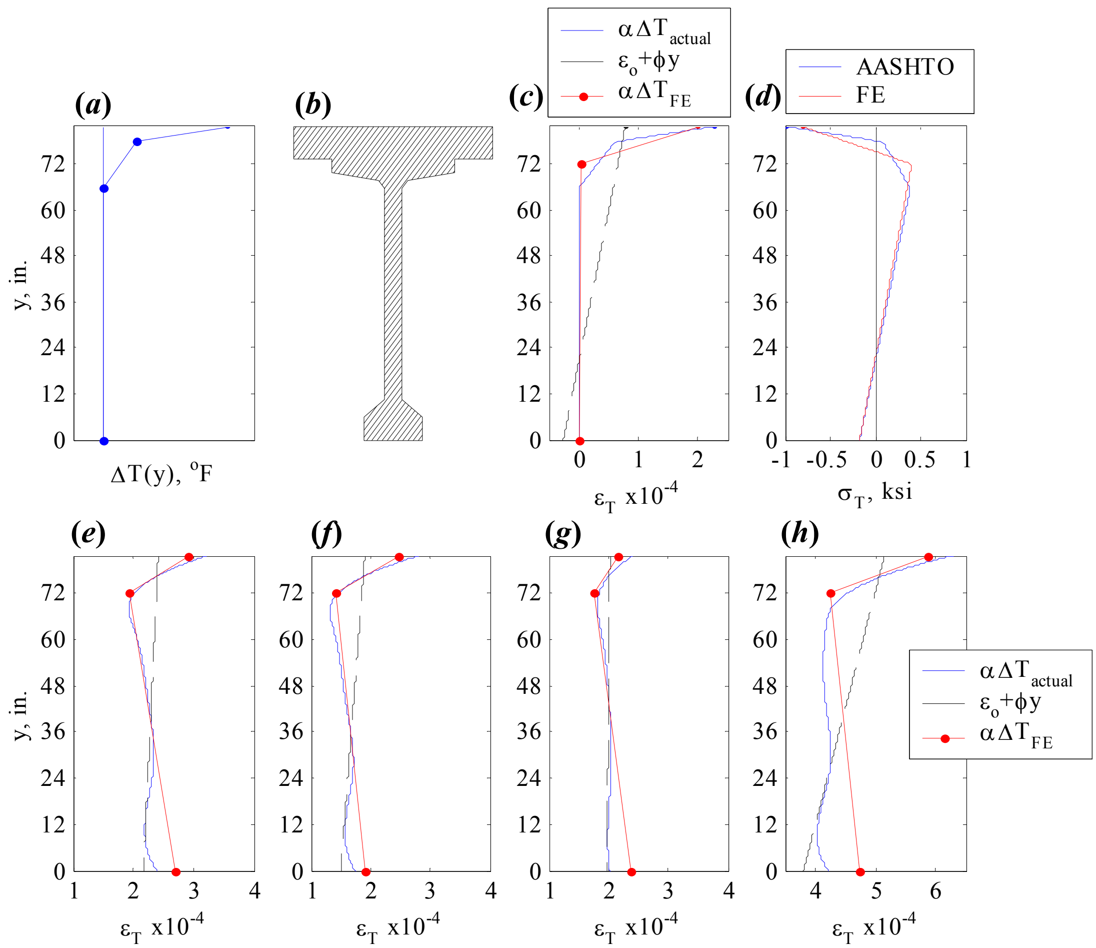

Fig. 13 – (*a*) Design thermal gradient[12]; (*b*) transformed composite girder section; (*c*) thermal strain due to theoretical and equivalent FEM thermal gradient, and resulting deformation strain; (*d*) thermal stress due to nonlinear thermal gradients; (*e*-*h*) thermal strain for select cases of measured thermal change

LIVE LOADING OF DECK

For studying the effect of live load, the TDOT standard truck HH32 shown in Fig. 16 (with rear and middle axle loads of 25.9 kips each and front axle load of 18 kips), which was used in actual load test of the bridge[18], was used in the ANSYS model as well. The load was placed on east (or instrumented) span with rear axle at 72 ft from the abutment and center right wheel at 2ft from the parapet curb. The resulting deformed shape of the bridge is shown in Fig. 17. The midspan deflection of the exterior girder was found to be 0.25", which agreed with the test data. The maximum span moment was found to be 500'k (677.5 kN-m), which again agreed with the test data. Negligible end slope changes also agree with test observations.

RESULTS

The 3D finite element model was subjected to five cases of thermal loading, including one theoretical case using the AASHTO (1998)-proposed temperature gradient, and four cases of temperature variation observed in service. In all cases, the gradient is markedly nonlinear near the top of the superstructure. The most extreme Case 4 is the difference between the most extreme high and the most extreme low events of temperature encountered. Corresponding to the level of strain reported in Fig. 13 (*h*), the temperature change at the top of the deck is 110ºF (43ºC). Fig. 14 shows the amplified deformed shape of the model, subject to the design thermal gradient. It can be seen from the figure that the pier does indeed deform with the superstructure, while allowing differential rotation for the pier diaphragm. This behavior was also observed through digital tiltmeter readings taken at the pier/diaphragm/girder interface periodically under different thermal conditions. It is also interesting to note that the smaller abutment on the west side undertakes virtually all of the deformation imposed on the structure. With two equal spans, and evenly distributed loading, it becomes obvious that this is due to the difference in size between the two abutments. It is believed that the difference in surface area between the two abutments results in an imbalance in terms of passive resistance behind the two abutments. It must be mentioned also that the backfill around the top of the piles is more flexible for the shallower abutment, as it is closer to the surface. This fact may help to explain why the taller east abutment, though it undergoes very little translation, shows more rotation than its smaller counterpart.

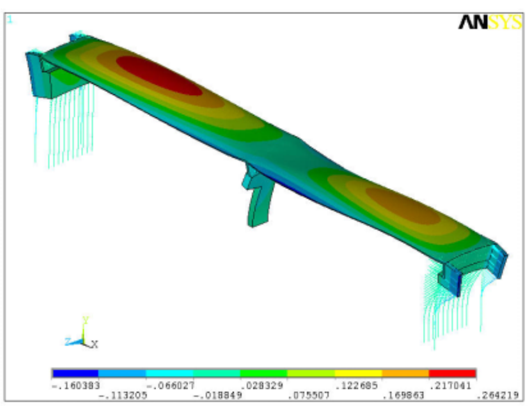

Fig. 14 Magnified Deformed Shape of Bridge Under Design Thermal Loading

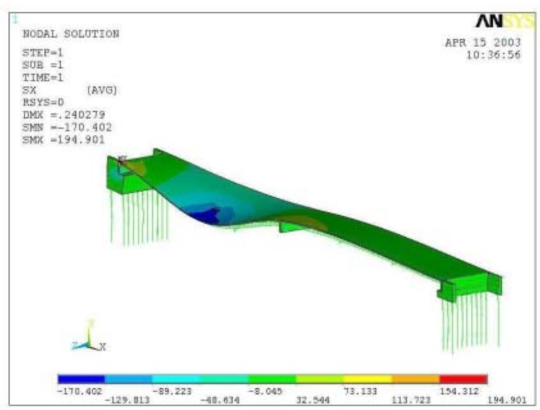

15. Magnified Deformed Shape Due to Truck Loading on Bridge

Deflection of the back wall, abutment, and pile for both integral abutments at bridge centerline is shown in Fig. 18 for all thermal cases studied. The tendency for the smaller abutment to take the majority of the deformation is again evident. The rotation of the larger abutment is also visible in the increasing deflection toward the top, whereas the smaller abutment is seen to resist rotation. Fig. 19 presents the moment diagrams for the middle pile from both abutments for the thermal cases studied. Moment in the west abutment piles is about ten times that in the east abutment piles. The maximum pile moment found for the most extreme thermal event corresponds to a bending stress of 12 ksi (85 MPa). The piles are more than adequate to undertake stresses of this level.20

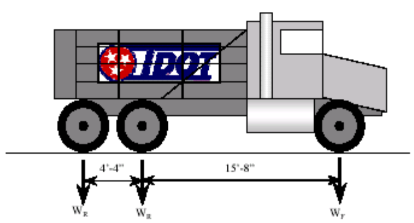

Fig. 16 TDOT HH32 Truck

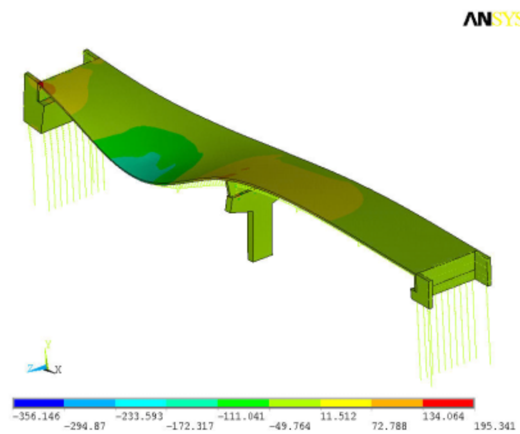

Fig. 17 Deformed Shape of Bridge Under Truck Load

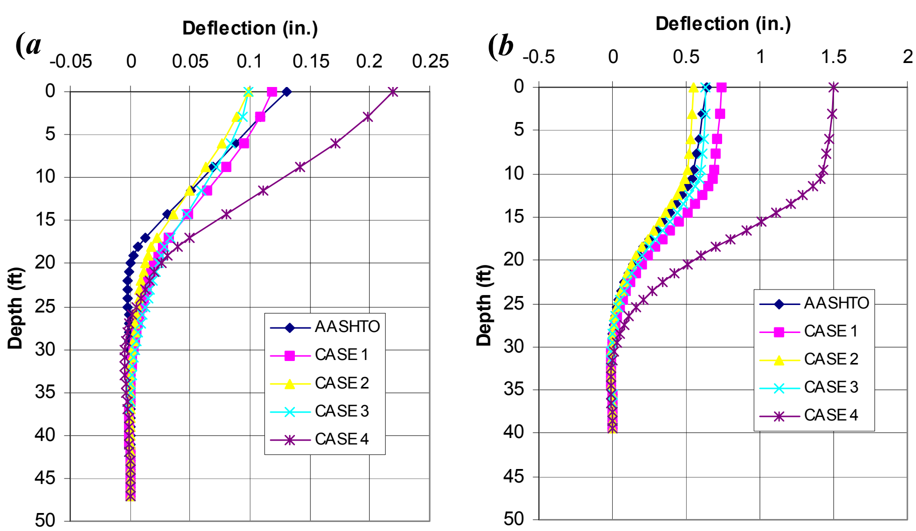

Fig. 18 Deflection of (a) East and (b) West Abutments due to Theoretical and Observed Thermal Gradients

CONCLUSIONS

One-dimensional representation of three-dimensional behavior of pretensioned concrete girder as part of a complete bridge system is possible if the critical features are included. ANSYS provided the necessary capability to do so. The three-D model of the bridge system considered in this study exhibited the behavior under different external influences quite accurately, as evidenced by close agreement with actual test data from field tests. This model can be used quite effectively for studying the effect of various parameters on bridge behavior. A very important aspect of integral bridge construction is the soil-structure interaction occurring at the abutments and supporting piles. The Winkler model involving

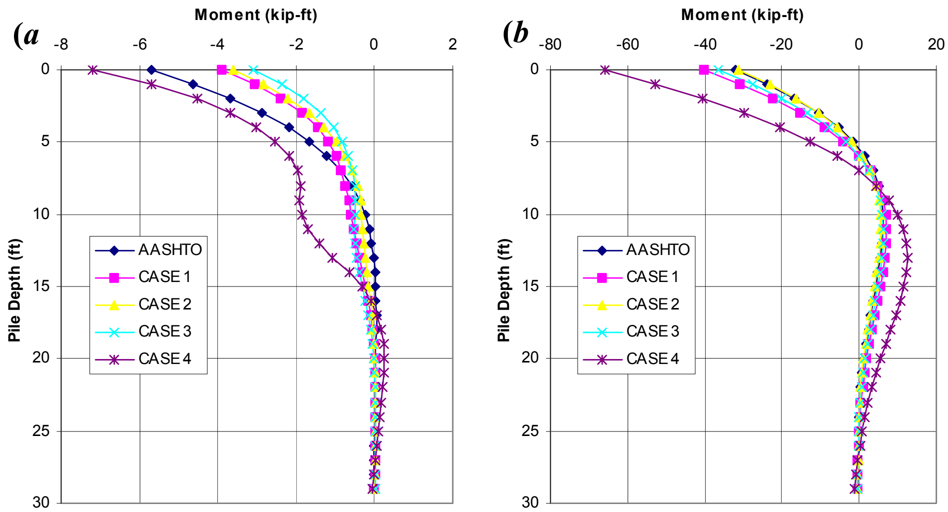

Fig. 19 Pile Moments at (a0 East and (b) West Abutments due to Theoretical and Observed Thermal Gradients

nonlinear equivalent spring behavior was successfully modeled, with consideration for variation in magnitude of stiffness with depth. A better representation of the pile-soil-pile interaction may be an interesting improvement. Solid elements with smeared reinforcements for concrete including cracking and crushing capabilities were used throughout the bridge except the pretensioned girders, which were modeled using beam elements. Under large enough external influences such a model would allow monitoring of damage due to cracking and crushing of concrete. However, the external influences considered so far did not cause any such damage in the structure. To monitor damage to the girders would have required modeling with similar solid elements but that would have increased the computational effort by an order of magnitude. The predicted thermal response under nonlinear temperature gradients exhibited good agreement with observed behavior of the bridge. Live load results showed excellent agreement with test data.

The model was found to be adequate in dealing with the complex analysis of integral bridges. It was found that the piles are sufficiently designed to undertake extreme thermal events. Also, it was found that the relative sizes of the abutments have a considerable effect on the deformation behavior of the structure. Effect of different pile lengths needs to be looked into. In this ongoing study, the finite element model will be used in studies of the effect of skew on integral bridge behavior, and further live load studies in particular. Work will be undertaken to construct simplified models as design tools to relieve some of the complexity of the design and analysis of integral bridges.

RECOMMENDATIONS

The analysis model to be used may range from very simple to very sophisticated. The simplest model may treat a girder along with its share of deck slab as a simple or continuous beam with horizontal and rotational spring supports at the ends., providing elastic or inelastic horizontal restraints at the ends. This will require appropriate assignment of spring properties based on studies with sophisticated models. A more sophisticated model of the bridge, that is the one used in this study will have the following features.

1. The pretensioned girders can be modeled by elastic beam elements (BEAM4) with the prestressing strand represented by tension or link elements (LINK8) following the centroidal line of the strands. The strand elements are then connected to the beam elements at the nodal points by means of vertical rigid link elements. The prestressing is defined by initial strain in the strand element with allowance being made for development length at the ends. If the objective is to determine bridge response due to thermal effects and live loads, it is not necessary to model the strands. On the other hand, if the inclusion of prestress as well as creep and shrinkage effects is important, the strand elements should be used.
2. The deck slab can be modeled by solid concrete elements (SOLID65) which accounts for the presence of reinforcing steel as well as accounts for cracking and crushing capability of concrete. To effect continuity between the deck slab and the girders, vertical rigid link elements connecting the beam nodes and slab nodes should be used.
3. The abutments, wing walls, diaphragms, and piers may also be modeled by solid concrete elements.
4. The steel HP piles supporting the abutments and pier can be conveniently modeled by thin-walled plastic beam elements (BEAM24).
5. The effect of earth pressure from foundation and backfill material on abutments and piles can be represented by nonlinear Winkler spring model based on suitable data (say, NCHRP data). The nonlinear spring element to be used for this purpose is COMBIN39.
6. Creep and shrinkage strain effects can be modeled indirectly by introducing these as initial strain effects.

The above model is suitable for studying bridge behavior under service loads. If, however, it is desired to study the response of the bridge with a progressive increase of magnitude of external effects (like live loads and temperature change) till collapse, a more sophisticated model with the girders modeled by solid concrete elements, the strands as well as primary unstressed steel modeled by appropriate link elements allowing for bond-slip and harped strands can be used. In this case, however, the size of the model will increase significantly and a nonlinear analysis involving significant computational effort may be in order.

REFERENCES

1. Sirisak, S., Basu, P.K., Spencer, E., " Evaluation of Bridge Structures Using ANSYS," *Computer Aided Engineering in 21st Century*, Proc. of 7th International ANSYS Conference, May 20-22, 1996, Pittsburgh, pp. 1.139-1.147.

2. ANSYS*, Reference Manual and Analysis Guide*, Version 6.1, ANSYS, Inc., Southpoint, 275 Technologty Drive, Canonsburg, PA 15317.

3. ASCE Task Committee on Concrete and Masonry Structures, ASCE State of the art report on finite element analysis of reinforced concrete, *ACI Journal*, Vol. 76, No.3, 1979, pp.

4. Willam K.J., and Warnke E. P.. Constitutive model for the triaxial behavior of concrete. *Proc International Association of Bridge and Structural Engineering*, Vol. 19, ISMES, Bergamo, Italy, 1975, pp.1-30.

5. Chen, W.F., *Plasticity in Reinforced Concrete*, McGraw-Hill Book Co., 1982

6. Arafa, M., and Mehlhorn, G., A modified discrete model in the nonlinear finite element analysis of prestressed and reinforced concrete structures*, 2nd PhD Symposium in Civil Engineering*, Budapest, 1998.

7. Lutz, L. A., and Gergely, P., ''Mechanics of bond and slip of deformed bars in concrete.'' *ACI Journal.,*Vol.64, No.11, 1967, pp. 711-721.

8. Ngo, D., and Scordelis, A. C., ''Finite element analysis of reinforced concrete beams.'' *ACI Journal,* Vol.64, 152–163, 1967.

9. ABAQUS, *Standard User's Manual and Theory Manual*, Version 6.3, Hibbit, Karlsson & Sorensen, Inc., 1080 Main Street, Pawtucket, RI 02860

10. ADINA, *Theory and Modeling Guide*, Report ARD 90-8. ADINA6 Users Manual, Report ARD 90-4. ADINA R & D Inc.

11. de Witte, F. C. and Kikstra, W. P., *DIANA R7.2 User's Manual, Nonlinear Analysis*, TNO Building and Construction Research, Delft, The Netherlands, 1999

12. AASHTO, LRFD Bridge Design Specifications, Second Edition, 1998.

13. Mitchell, D., Cook, W. D., Khan, A. A., and Tham, T. (1993). "Influence of High Strength Concrete on Transfer and Development Length of Pretensioning Strand." *PCI Journal*. 38(3), 52-66.

14. National Cooperative Highway Research Program (NCHRP). (1991). Manuals for the Design of Bridge Foundations. R. M. Barker, J. M. Duncan, K. B. Rojiani, P. S. K. Ooi, C. K. Tan, and S. G. Kim. Eds. Rep. 343, Transportation Research Board, Washington, DC.

15. Bransby, M.F., and Springman, S., "Selection of load-transfer functions for passive lateral loading of pile groups," Computers and Geotechnics, Vol.24, 1999, pp.155-184.

16. S.K. Padmarajaiah, S.K., and Ramaswamy A., A finite element assessment of flexural strength of prestressed concrete beams with fiber reinforcement. Cement & Concrete Composites 24 (2002) 229–241

17. Imbsen, R. A., Vandershaf, D. E., Shamber, R. A., and Nutt, R. V., Thermal Effects in Concrete Superstructures. *NCHRP Report No. 276,* Transportation Research Board, Washington, DC, 1985

18. Basu, P.K., and Knickerbocker, David, High Performance Concrete Bridges, Final report of TN DOT Project No. TNSPR-RES1162, Vanderbilt University, March 2002.